Study and Selection of Parameters of Automatically Controlled Wind Power Station with Swaying Sails

Korganbay Sholanov*, Aibek Kabanbayev*‡, Kuanysh Abzhaparov**

* Production Processes Automation Department, Faculty "Energy, Automation and Telecommunication", Karaganda State Technical University, 56 N.Nazarbayev av., Karaganda 100027 Republic of Kazakhstan

**Automation and Control Department, A. Burkitbayev Institute of Industrial Automation and Digitalization, Satbayev University, 22a Satbayev Str., Almaty 050013 Republic of Kazakhstan

(sholkor@gmail.com, jogitama@gmail.com, koli-87@mail.com)

‡ Corresponding Author; Aibek Kabanbayev, 56 N.Nazarbayev av., Karaganda 100027 Republic of Kazakhstan, Tel: +7 7078513031, jogitama@gmail.com

Received: 26.02.2020 Accepted:04.04.2020

Abstract- Related to the use of the traditional energy sources, environmental pollution and global warming are the reasons of the growing interest to the development of the renewable energy, and in particular, wind energy. Wind energy development includes solving the problem of increasing efficiency of wind energy conversion and expending the territory of wind power stations (WPS) spread. Unfortunately, the existing mainly turbine WPS are located only at the territories with strong winds, as their efficiency dramatically decreases with the decrease (below 10 m/s) of the wind speed.

This article studies a new sail wind power station with low capacity that allows effective conversion of the wind energy and expansion of the territory of the WPS use due to the possibility to effectively generate electric current with the wind speed of 2.5 m/s and higher. This possibility is achieved due to automated control of the sail surface area having toroidal shape, and due to the use of controlled damping system consisting of the parallel manipulator. We have carried out experimental and computer studies of aerodynamic features of different sails; according to the results of these studies we have chosen the toroidal shape and profile of the air-inflated sail section. To confirm the functional capabilities of the new WPS, we have created the demonstration model. Using the automatic control theory, the paper develops the mathematical apparatus that allow calculating and selecting the main parameters of the sail WPS.

Keywords wind power station, toroidal sail, dynamic model, parallel manipulator, spatial damper, control system.

1. Introduction

The possibility of wind sources of the renewable energy to generate electric current at any point of land surface and coastal area of water space make wind power station a promising segment of the global energy. The emerging at the moment trend of transition from hydrocarbon energy sources to renewable energy further increased commitment of the community to the improvement and introduction of new renewable sources such as wind power stations. However, age-long experience of using wind power stations shows [1] that the efforts of scientists, engineers and power engineers are focused primarily on improving the efficiency of the wind energy conversion in the equipment of turbine WPS. It is known that turbine WPS are divided into WPS with the horizontal and vertical orientation of the turbine axis [1, 2]. And in the WPS with the horizontal axis orientation, the turbine rotor blades move under the lifting forces

of the wind applied to the blades [3]. Functioning that does not depend on the wind direction changes distinguishes the WPS with a vertical orientation of the turbine axis which mainly works due to forces of resistance to the airflow [4,5]. However, as is seen from the researches and many years of the operation experience [1,6-8], for turbine WPS of both types, the main problems are created by the unpredictability of the wind, its speed and gust force, frequently changing timespans. Also, the problem is that the lower limit of the wind speeds range, with which the turbine WPS operate with the rated power, is usually quite high, more than 10 m/s with a maximum efficiency of 0.3 [9]. In this regard, in immense territories with an average wind speed of 3 m/s, turbine WPS cannot be used. To solve the problem of improving turbine WPS, optimal wind converters are searched for [10], turbine WPS design is constantly modified [11-12]. It should be noted that, despite the enormous efforts aimed at improvement, in power production by turbine wind power generator still has a lot of flaws and problems [13]. In this regard, new solutions are of interest in wind energy aimed at fundamental change of the design of WPS, namely the rejection of the rotating turbine and creation of sail WPS. Practice of using sails, for example, for ships has shown that yachts can move at speeds that exceed the wind speed [14], at the same time, methods for calculating sails [15] have been developed for sea-craft. For the first time, pilot design of a sail WPS [16] without the rotating turbine was developed by the Tunisian startup Saphon Energy. However, mainly due to additional dynamic loads caused by the elastic oscillation of the mast and inefficiency of functioning, this sail WPS did not gained wide use in practice. A sail wind generator that swings due to aeroelastic resonance phenomena created by the airflow in the direction that is perpendicular to the main flow, is described in work [17], however, this generator having a low capacity is still at the development stage. The new sail WPS proposed in works [18,19], has a toroidal sail that moves cyclically under the lift force and wind resistance. The structural specifics of this WPS is that the motion of its working body (WB) consisting of the sail, mast and moveable platform of the manipulator is transmitted to actuators of the six-degree-of-freedom parallel manipulator SHOLKOR [20], which converts these movements into six translational movements. In the future, the energy of translational movements can be converted through the power take-off system into electrical energy.

This article continues the research of this sail WPS and includes: substantiation of the sail shape and section; creation of a better dynamic model; use of parallel manipulator in addition as an active controlled damping system; WPS control by changing the value of the damping force (preload).

2. Study and Selection of the Sail Shape and Section

2.1. Computer Study of the Sail Shape

To justify the sail shape, we have conducted computer simulation of the aerodynamic spectrum of the ball with diameter D = 400 *mm* (Fig. 1, *a*) and a torus of equal volume (Fig. 1 *(b),* show the side flowing of the torus) with an air flow moving at a speed of 10 m/s.

(a)

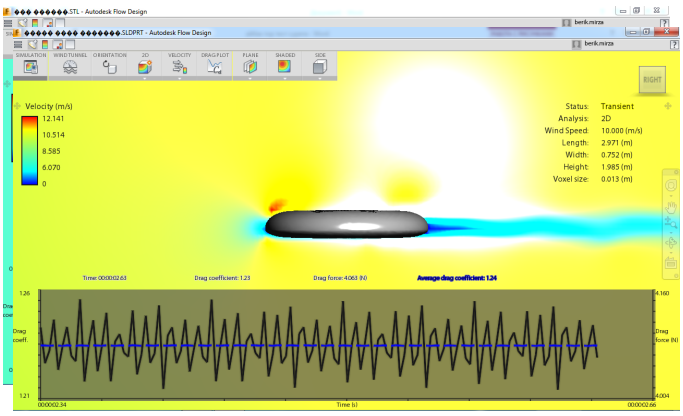

(b)

Fig.1.Aerodynamic spectra of the sail models

Thus, the aerodynamic spectra obtained with the help of the AutodeskFlowDesign program showed that the head drag coefficients of the ball and the torus equal to c_c=*0.44* and c_t= *1.24*, respectively. According to the flow pattern, it is seen that there are 2 sections on the upper surface of the torus and the ball with an increased jet velocity. Moreover, the jet velocity on the upper surface of the torus is higher than that of the ball. Based on the obtained aerodynamic spectra, it can be concluded that the drag and lift forces act simultaneously on the toroidal sail, and these forces have greater value

than the aerodynamic forces acting on the ball. Hence, the sail with the torus shape excels the spherical sail shape in terms of its aerodynamic characteristics. Besides, selection of the toroidal sail ensures the airflow breakdown at certain angles of attack and thereby enables the WB perform cyclic movements.

2.2.Experimental Study of Aerodynamic Forces Acting on Toroidal Sails

Aerodynamic features of linear bodies with such a cross-section profile have been studied sufficiently, for example, in aircraft construction. The set of the aircraft wing sections forms a linear body of a cylindrical (conical) shape in the form of a straight line. In the toroidal sail, the generatrix surfaces are circles. The aerodynamic features of toroidal bodies with the aerodynamic profile of the section have not been studied. In this regard, experimental studies of the toroidal sail with the aerodynamic profile were performed in the wind tunnel.To conduct aerodynamic testing, three models of the toroidal sail were made of expanded polystyrene, with the following dimensions: outer diameter D_1 = 500 mm, D_2= 450 mm, and D_3 = 400 mm; internal diameter d_1 = 126 mm, d_2 = 112 mm, and d_3 = 100mm; height h_1 = 70 mm, h_2 = 64 mm, and $h3$ = 56 mm. Cross section of all toruses corresponds to the aerodynamic profile of NASA - 2210 [21].During the experiment, for the three dimensions of toroidal sails, lifting and resistance forces were determined at different wind speed and angle of attack. Therewith, the wind speed varied from 3 to 20 m/s, and the angle of attack from 0^0 to 20^0.According to the processed data, the graphs were built are regularities were revealed for all three dimension types. To illustrate this, Figure 2 for the bigger sail gives diagrams of lift *(a)* and

$$S = \frac{2N}{\eta \cdot \rho \cdot v_W^3}. \qquad (1)$$

Here ρ is the air density. The preliminary calculation is made on the minimum wind speed equal to v_W = 2.5 m/s. Roughly, the efficiency factor is taken equal to η = 0.5.If the sail

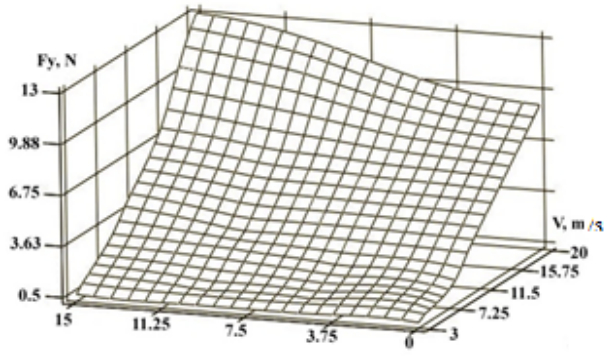

drag *(b)* force dependency on wind speed and angle of attack. According to the results of computer simulation and experiments, the following conclusions may be made: when the airflow flows around the toroidal sail, drag and lifting forces appear; lifting force is higher than drag forces; aerodynamic forces grow with speed and angle of attack; aerodynamic forces grow with the increase of geometrical dimensions of the sail; with low wind speeds, the effect of the angle of attack on the aerodynamic forces is insignificant.

(a)

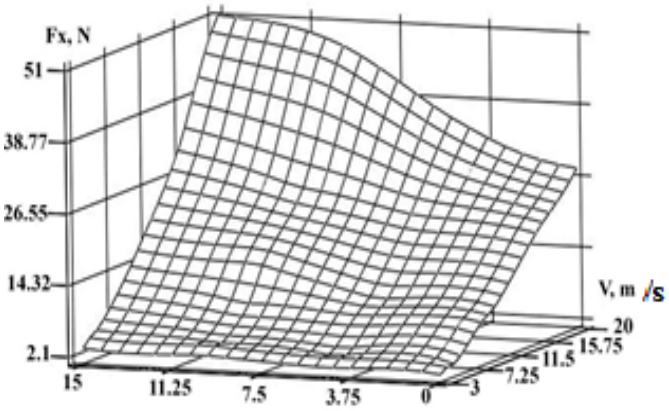

(b)

Fig.2. Graphs of lift force *(a)* and drag force *(b)* dependence on the wind speed and angle of attack with diameter D_1=500 mm.

3. Analysis of the WPS Dynamics

3.1. Dynamic Analysis of the WPS Working body

When building a simplified dynamic model of the WB, the sail is taken as a rigid body. The maximum value of the sail surface area is set according to the required capacity N for the WPS [22]
dimensions appear to be unacceptably large, then several sails are chosen so that the sum of their surface areas matches the required value. In paper

[19], it was established that the toroidal shape of the sail enables the airflow breakdown when the mast is inclined at an angle of $\beta \sim \pm 10^{\circ}$. Thus, previously generated [19] dynamic model was improved by the use of equations of the state. Obtained dynamic model allows obtaining forces effecting on the manipulator for determining the controlled damping efforts. After that, the movement of the WB's sail under the action of the

wind is taken as the forward stroke and the movement under the damping forces as the return stroke.WPS parameters and control systems are calculated based on the condition that the deviation of the WB mast from the vertical position at the forward stroke does not exceed the angle β. Figure 3 presents the design model of the WPS consisting of bottom 1 and upper 2 platforms of the manipulator connected by the actuators 4-8 by flexible cable bonds:9 – made of two links; 10 – made of three links; 11 – made of four links. The mast 12 rigidly connects the sail 13 with the upper platform 2 of the manipulator. To analyze the WB dynamics, we set two coordinate systems. The fixed coordinate system $C_1X_0Y_0Z_0$ is related to the fixed platform 1 of the manipulator, the axis C_1Z_0 is directed vertically upward, and the axis C_1Y_0 is directed along the edge C_1A_1.The movable system $O_{01}X_{01}Y_{01}Z_{01}$coincides with the center of the movable platform in the initial position O_{01}.The $O_{01}Z_1$ axis is parallel to the C_1Z_0 axis. To build a mathematical model, it is supposed that the WB motions occur in the Q plane (Fig. 3), coinciding with the $Q_{10}Y_1Z_1$ plane where the resulting vector F_W of the wind force and O_1O_r axis of the WB mast are located. The vertical F_1 and horizontal F_2 compounds of the wind force, the gravity G act in the Q plane and cause the plane motion of the WB in the $Q_{10}Y_1Z_1$ plane. The position of the $Q_{10}Y_1Z_1$ plane depends on the direction of the wind speed and is determined by the angle α between the axes C_1Y_0 and the axis $O_{01}Y_{01}$.During plane-parallel motion, the WB moves in the $O_{01}Y_1Z_1$ plane and rotates around the SX^1_1 axis that is parallel to the $O_{01}X_1$ axis. Mass center S of the working body is located on the O_1Z_1 axis at the distance of $O_1S = L_S$. When forming the mathematical model of the WB, we take into account the fact that this model is later used to determining damping forces in the parallel manipulator.

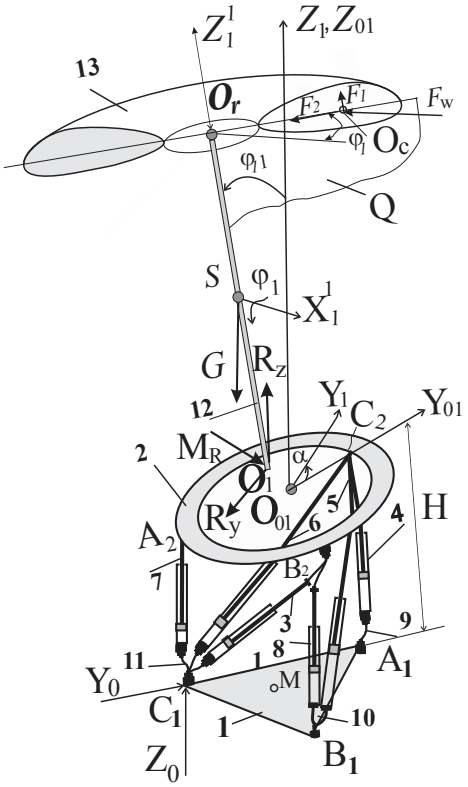

Fig.3.Design model of the WPS

In this regard, dynamic equations are made on the form of the state equations. Parameters of the state are represented by the vectors $X_1=[X_{11}\ X_{12}\ X_{13}]^T=[y_S\ z_S\ \varphi_1]^T$ and speed vector $X_2=[X_{21}\ X_{22}\ X_{23}]^T=[\dot{y}_S\ \ \dot{z}_S\ \ \omega_1\ ]^T$, where ($y_S$, z_S) are coordinates of the mass center.equation of the dynamics during the forward stroke is

$$\dot{\mathbf{X}}_1 = \mathbf{X}_2,$$
$$\dot{\mathbf{X}}_2 = \mathbf{M}^{-1}[\mathbf{D}(\mathbf{X}_1)\frac{1}{2}\rho S_P {v_W}^2 - \mathbf{F}(\mathbf{X}_1)]. \quad (2)$$

Working body in the fixed system $O_{01}X_{01}Y_{01}Z_{01}$; φ_1 - angle of rotation of the working body as related to axis SX^1_1 .The matrix Here v_w is mathematical expectation of the wind speed with a pulsating load, S_P is surface area of the toroidal sail (sails), ρ is air density, $\mathbf{M^{-1}}$ (3x3) is inverse inertia matrix equal to

$$\mathbf{M}^{-1} = \begin{pmatrix} 1/m & 0 & 0 \\ 0 & 1/m & 0 \\ 0 & 0 & 1/J_{SX} \end{pmatrix}. \quad (3)$$

The coefficient of the summarized force from the wind effect is determined by the matrix **D** (3x1)

$$\mathbf{D}=\begin{pmatrix} c_A \operatorname{Sin}(X_{13})+c_W \operatorname{Cos}(X_{13}) \\ c_A \operatorname{Cos}(X_{13})+c_W \operatorname{Sin}(X_{13}) \\ c_A \cdot O_r O_c + c_W \cdot O_r O_s \end{pmatrix}, \quad (4)$$

where the constants c_A, c_W show experimentally established lift coefficients, of the lifting force F_1 and drag force F_2 for the selected section of the sail with the aerodynamic profile. $\mathbf{F}(\mathbf{X})(3x1)$ is the summarized force of the G gravity force, R_Y, R_Z reaction forces and M_R reaction force moment expressed using the matrix

$$\mathbf{F}(\mathbf{X}_1)=\begin{pmatrix} R_Y \\ R_Z - G \\ O_1 S(R_Y \operatorname{Cos}(X_{13})+R_Z \operatorname{Sin}(X_{13}))+M_R \end{pmatrix} \quad (5)$$

The working body forward stroke finishes at the angle of $\varphi_1=\beta$ and the return stroke starts at an angle of β - φ_1, where $0 \le \varphi_1 \le 2\beta$. The return stroke occurs under the effect of damping forces, and the minimum wind effect resists the WB movement. Therefore, the dynamic equation changes: in the second equality (2), the right side is multiplied by (-1). Thereby, it is sufficient to derive the necessary dependencies as exemplified by the forward stroke. It is not difficult to obtain such derivations for the reverse stroke due to the small difference in the dynamic equations. Let us transform the second equation (2) into a form convenient for establishing the reaction forces depending on the state parameters. We assume state parameters as input variables, and variable reaction forces as output. Let us consider the initial unstable equilibrium position when the mass center of the WB takes its initial position. This position (M) is the operating point on the mass center path. At the same time, the higher is the mass center from the ground, the higher the speed, because the wind speed gradient increases according to the Hellman exponential law [23]. The change in the state vector causes the change in the reaction forces, which follows from the dependencies given below obtained by substituting expressions (3-5) into the second matrix equality (2).

$$R_Y = G_1(\mathbf{X}) = -m\dot{X}_{21} + [c_A \operatorname{Sin}(X_{13}) + c_W \operatorname{Cos}(X_{13})] \cdot \frac{1}{2}\rho S_P v_W{}^2,$$
$$R_Z = G_2(\mathbf{X}) = -m\dot{X}_{22} + [c_W \operatorname{Sin}(X_{13}) + c_A \operatorname{Cos}(X_{13})] \cdot \frac{1}{2}\rho S_P v_W{}^2 - G. \quad (6)$$
$$M_R = G_3(\mathbf{X}) = -J_{SX}\dot{X}_{23} + [c_A \cdot O_r O_c + c_W \cdot O_r O_s] \times \frac{1}{2}\rho S_P v_W{}^2 - O_1 S[R_Y \operatorname{Cos}(X_{13}) + R_Z \operatorname{Sin}(X_{13})] \cdot \frac{1}{2}$$

To solve the system of equalities (6), let us use the method of tangent approximation [24], taking into account that near the M operating point the mass center path represents a continuous curve. Then small deviations (incrementations) of the reaction forces corresponding to the incrementations of the state parameters are determined by the ratio

$$(\Delta R_Y \quad \Delta R_Z \quad \Delta M_R)^T = \mathbf{J}_{36}(G)|_M \times \times (\Delta X_{11} \quad \Delta X_{12} \quad \Delta X_{13} \quad \Delta X_{21} \quad \Delta X_{22} \quad \Delta X_{23})^T \quad (7)$$

where Jacobian matrix in the operating point M is

$$\mathbf{J}_{36}(G)|_M = \left.\begin{pmatrix} \frac{\partial G_1}{\partial X_{11}} & \cdots & \frac{\partial G_1}{\partial X_{23}} \\ \frac{\partial G_2}{\partial X_{11}} & \cdots & \frac{\partial G_2}{\partial X_{23}} \\ \frac{\partial G_3}{\partial X_{11}} & \cdots & \frac{\partial G_3}{\partial X_{23}} \end{pmatrix}\right|_M \quad (8)$$

In the equations (6) it is assumed that the state parameters (kinematic characteristics) are given reasoning from that the working body performs plane-parallel movement.Based on the values of the state parameters in the working point of the dependencies (7),values of the components of the WB reaction forces are determined at the working point

$$R_{Y0}|_M = -m\dot{X}_{21} + c_W \cdot \frac{1}{2}\rho S_P v_W{}^2,$$
$$R_{Z0}|_M = -m\dot{X}_{22} + c_A \cdot \frac{1}{2}\rho S_P v_W{}^2 - G, \quad (9)$$
$$M_{R0}|_M = -J_{SX}\dot{X}_{23} + [c_A \cdot O_r O_c + c_W \cdot O_r O_s] \cdot \frac{1}{2}\rho S_P v_W{}^2 - O_1 S \cdot R_{Y0}|_M .$$

Reaction forces R_Y, R_Z, M_R follow as totals

$$R_Y = R_{Y0}\,|_M + \Delta R_Y,$$
$$R_Z = R_{Z0}\,|_M + \Delta R_Z, \qquad (10)$$
$$M_R = M_{R0}\,|_M + \Delta M_R.$$

Taking into account (7-10) we will get the equations for calculating reaction forces in the form

$$R_Y = G_1(\mathbf{X}) = R_{Y0}\,|_M + [c_A \operatorname{Cos}(X_{13}) - c_W \operatorname{Sin}(X_{13})]\Delta X_{13} \cdot \frac{1}{2}\rho S_P v_W{}^2,$$
$$R_Z = G_2(\mathbf{X}) = R_{Z0}\,|_M + [c_W \operatorname{Cos}(X_{13}) - c_A \operatorname{Sin}(X_{13})] \cdot \Delta X_{13} \cdot \frac{1}{2}\rho S_P v_W{}^2. \qquad (11)$$
$$M_R = G_3(\mathbf{X}) = M_{R0}\,|_M + O_1 S[R_Y \operatorname{Sin}(\varphi_1) - R_Z \operatorname{Cos}(\varphi_1)]\Delta X_{13}.$$

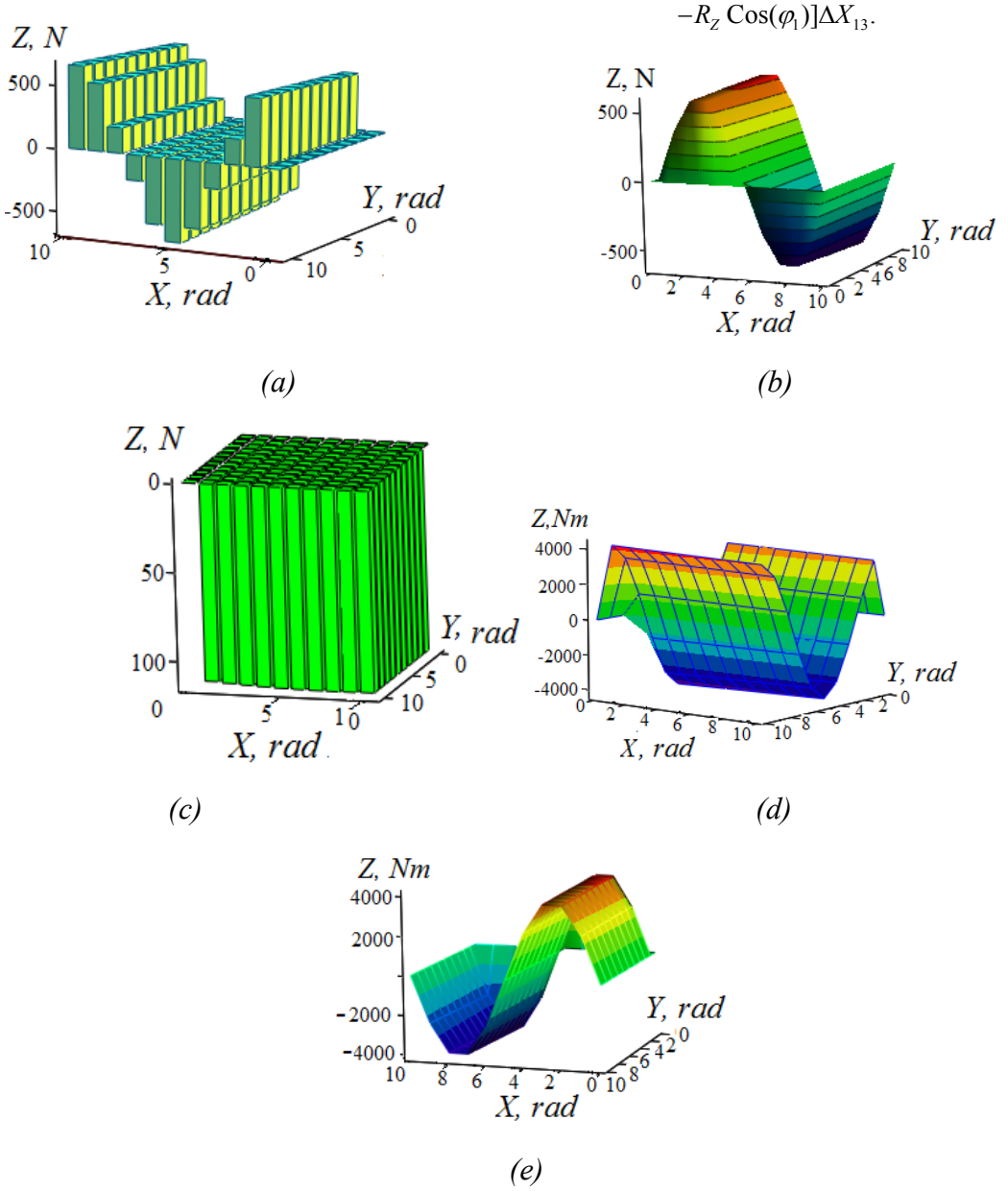

Fig.4. Graphs of variance of the projections on the motionless axes of forces and reaction forces moments depending on the wind direction and mast inclination angle.

These forces and inertia reaction torque will in the future allow identifying efforts on actuators and spring dampers. Based on the obtained algorithm, a program was designed in the Mathcad and projection of the reaction forces are determined for motionless coordinate axes presented in Figure 4.As incoming data it is accepted that WPS

capacity is 1 kW, wind speed is 3 m/s, mast length is 10 m, and working body weight is 120 kg.

Figure 4 shows the graphs of dependence on the wind direction *(α)* and rotation angle *(φ)* of the working body, projections of the following values: force R_Y on axis $O_{01}Y_{01}$*(a)*; force R_Y on axis $O_{01}X_{01}$ *(b)*; force R_Z on axis $O_{01}Z_{01}$ *(c)*; reaction force moment M_R on axis $O_{01}X_{01}$ *(d);* reaction force moment M_R on axis $O_{01}Y_{01}$ *(e).* At the same time, on the *X axis,* angle $\alpha = k \cdot \pi / 18$ *(k =1÷10)* of wind direction is depicted in radians, through π/18; on the *Y* axis angle $\varphi = i \cdot \pi / 180$ *(i=1÷10)* of the WB rotation is depicted in radians, through π/18.The analysis of the graphs allows making the following conclusions: the lifting force decreases the reaction caused by gravity forces (Fig.4,c); rotation angle alteration changes the forces and moments of reaction forces; change of the wind direction effects the forces and moments; the greatest amount of the energy is transferred during swinging (Fig.4,*d*,e).Indeed, if we take into account that the maximum angular speed of the working body swinging for a given wind speed ω=0.3 c^{-1}, it follows that swinging transmits approximate power of 1290 W in the form of mechanical energy, excluding the power of other reaction forces. This is above the given power of 1 kW that was used for determining the area of the sail surface according to the resistance force (1).Hence, it gives an important result stating that the conversion of wind energy into mechanical energy due to the lifting forces acting on the sail, extra energy is extracted. This fact confirms the advantage of the sail WPS in terms of wind energy conversion efficiency.

3.2. Analysis of the manipulator platform position

The following objective is to establish the position of the nodal points A_2,B_2,C_2 of the upper platform, if the position of the WB is set by the coordinates ($\Delta y_S \Delta, z_S$) of the center S and by the rotation ($_{\Delta\varphi 1}$) relative to the axis that crosses *S* perpendicularly to *Q* plane. Initial data are considered to be that the upper and bottom platform in present regular triangles with sides equal to *a*. Platform height in its initial position amounts to *H*. To solve this kinematic problem, we use homogeneous transformation matrix applied in robotics [25]. Previously chosen coordinate systems are used. The current position of the WB is presented with the help of mobile the trihedral prism SA_2,B_2,C_2.Based on the condition of selecting the auxiliary fixed coordinate system, it follows that in the platform initial position, coordinates A_2,B_2,C_2 are determined by the radius vectors

$$r_{A2} = \left(-a\frac{\sqrt{3}}{6} \quad -a/2 \quad 0 \quad 1 \right)^T, \; r_{B2} = \left(a\frac{\sqrt{3}}{3} \quad 0 \quad 0 \quad 1 \right)^T,$$
$$r_{C2} = \left(-a\frac{\sqrt{3}}{6} \quad a/2 \quad 0 \quad 1 \right)^T.$$

Rotation of the system $O_{01}X_{01}Y_{01}Z_{01}$ around the axis $O_{01}Z_{01}$ for the angle α are described by the homogeneous transformation matrix A_1^{01}. Then, coordinates of the junctions in the local system of coordinates $O_{01}X_1Y_1Z_1$ are determined from the equality

$$r_{A2}^1 = A_1^{01} r_{A2}, \;\; r_{B2}^1 = A_1^{01} r_{B2}, \;\; r_{C2}^1 = A_1^{01} r_{C2}, \tag{12}$$

To determine positions of the points of junctions of the upper platform and center O_1 in the $O_{01}X_1Y_1Z_1$ coordinates system, the following homogeneous matrixes are used: A_T, describing the transformation with parallel transfer of mobile system $O_1X_1^1Y_1^1Z_1^1$ for the value of Δy_s, Δz_s and shift for the value of L_S along axis $O_1Z^1{}_1$; A_R - rotation around axis $SX^1{}_1$for the angle $\Delta\varphi^i{}_1$; A_L - matrix of parallel transfer along axis $S_1Z_1^1$ for the value of $-L_S$. To determine positions of the points of junctions of the upper platform and center O_1 in the coordinates system $O_{01}X_1Y_1Z_1$ with slight displacements of the WB, the following transformation composition matrix is used

$$T_1^{11} = A_T \cdot A_R \cdot A_L.$$

Now the position of the points of junctions and the center O_1 of the platform in the local system $O_{01}X_1Y_1Z_1$ is determined based on the equation

$$\begin{aligned} &r_{A2}^{01} = T_1^{11} r_{A2}^1, \;\; r_{B2}^{01} = T_1^{11} r_{B2}^1, \;\; r_{C2}^{01} = T_1^{11} r_{C2}^1, \\ &r_{O1}^{01} = T_1^{11} \left(0 \quad 0 \quad 0 \quad 1 \right)^T. \end{aligned} \tag{13}$$

The coordinates of these points (13) in the fixed system $C_1X_0Y_0Z_0$ are

$$r_{A2}^0 = T_0^1 r_{A2}^{01},\ \ r_{B2}^0 = T_0^1 r_{B2}^{01},\ \ r_{C2}^0 = T_0^1 r_{C2}^{01}, r_{O1}^0 = T_0^1 r_{O1}^{01}, \quad (14)$$

where transformation matrix is

$$T_0^1 = \begin{pmatrix} 1 & 0 & 0 & b\sqrt{3}/2 \\ 0 & 1 & 0 & b/2 \\ 0 & 0 & 1 & H \\ 0 & 0 & 0 & 1 \end{pmatrix}.$$

A change in the position of the upper platform of the manipulator causes a change in the position, lengths of actuators, the direction of reaction forces vectors effecting the upper platform from the actuators. To determine these values, the inverse kinematics problem is solved for the manipulator. This problem [26] consists in that at a known position of the moving upper platform on coordinates of points of junctions (A_2, B_2, C_2), the orientation and lengths of actuators are established, hence the direction of actuators reaction forces acting along the axis of actuators. As an example, we will solve the inverse problem only for the actuator 6 (Fig. 5). The coordinates of the junction C_2 (x_{C2}^0 y_{C2}^0 z_{C2}^0) are known from the equation (14), the coordinates of the junction C1 (0 0 0) are equal to zero. The current length of the actuator 6 is equal to

$$l_{6t} = \sqrt{(x_{C2}^0)^2 + (y_{C2}^0)^2 + (z_{C2}^0)^2}\ . \quad (15)$$

Angles $\alpha_6, \beta_6, \gamma$between the axis of the actuator 6 and axesC_1X_0, C_1Y_0, C_1Z_0 of the fixed coordinate systems are determined as

$$\alpha_6 = arc\cos(x_{C2}^0 / l_{6t}),\ \ \beta_6 = arc\cos(y_{C2}^0 / l_{6t}) \quad (16)$$

$$\gamma_6 = arc\cos(z_{C2}^0 / l_{6t})$$

Change in the length of the actuator 6 is

$$\Delta l_6 = l_{6t} - l_6\ . \quad (17)$$

If angles $\alpha_6, \beta_6, \gamma_6$are known, then it is easy to determine reaction forces projections N_{6X}, N_{6Y}, N_{6Z} of actuator 6 (Fig.5) on motionless axes of coordinates. For other actuators, calculations similar to (15-17) are performed and actuator length change and their orientation in the motionless system of coordinates are determined.

3.3. Analysis of the damping system of the parallel manipulator

The figure 5, *a* shows the spatial damping system [27] consisting of parallel manipulator with spring dampers. Here, the fixed platform 1 and the moving platform 2 are connected by six spring dampers 3-8 combined with actuators. Moreover, these dampers and linked between themselves and with the platforms with the help of chain couplings [18] (cable bonds are also possible).To ensure feedback in the dampers' control system, each cylinder (guide) 9 has a displacement sensor 10 that measures the position of the rod relative to the cylinder.Figure 5 shows the fixed $C_1X_0Y_0Z_0$ and the moving $O_1X_1Y_1Z_1$ coordinate systems, previously selected. The reaction forces effecting the platform 2 from the side of dampers are directed along their axis. In order not to overload the drawing, the reaction forces N_6,N_7,N_8 are shown only for dampers 6, 7, 8.Moreover, the example of the reaction force N6 shows the projections of forces and angles, formed by each axis of a damper with the axes of the $C_1X_0Y_0Z_0$ system, known from the solution of the inverse problem (16) for each position of the manipulator. Each damper reaction forces consist of 3 forces, caused by the mass of the actuator and friction forces N_M ; spring elasticity $N_D=k\Delta l_d$; spring preload $N_C=kl_c$

$$N_n = N_{nM} \pm k \cdot \Delta l_{nD} \pm k \cdot l_{nc}\ \ (n\text{=}3\text{-}8).$$

The last summand (force NC=klc) changes in its size by the control system. Figure 6, b shows the scheme of a damper consisting of the rod 11 with a plunger 12 moving along the guide 13. Damping is carried out using the spring 14 with the stiffness coefficient (k).In the damper, the spring is compressed when the WB moves under the wind gust and when it is released, it returns the WB during the return stroke [28].The length of the spring (Fig. 6,b) in its free state is $l=lc+lt+\Delta l$, where lc is the controlled spring length change during preloading; lt is the length of the unstrained part of the spring; Δl is the value of spring deformation (17).

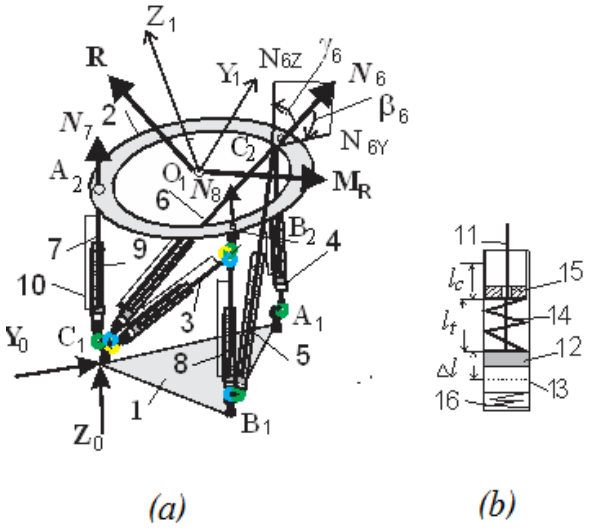

Fig. 5. Damping system

To evaluate the WPS power during designing generating system or operation, data on forces in actuators are required. Forces on the rod of cylinders enable to choose the structure of dampers. As the initial data, we use the main vector of the reaction force $\vec{\mathbf{R}} = \vec{\mathbf{R}}_{\mathbf{Z}} + \vec{\mathbf{R}}_{\mathbf{Y}}$ applied in the point O_1 and the vector of the pair of the reaction force $\vec{\mathbf{M}}_R$, obtained in dependencies (11) as a result of the dynamic analysis of the WB. It is worth noting that the force $\vec{\mathbf{R}}$ is located (Fig. 5) in the Q plane, and the moment vector of the forces couple $\vec{\mathbf{M}}_{\mathbf{R}}$ is directed perpendicular to the Q plane coinciding with the moving plane $O_1Y_1Z_1$.Thus, at the specified wind direction, the values $\vec{\mathbf{R}}$ and $\vec{\mathbf{M}}_{\mathbf{R}}$ are known.Virtually, reaction forces of actuators $\mathbf{N}_3$, $\mathbf{N}_4$, $\mathbf{N}_5$, $\mathbf{N}_6$, $\mathbf{N}_7$, $\mathbf{N}_8$, directed along the axes of the actuators, effect on the platform 2. Let us remind that the line of action directions of these forces for each position are determined by solving the inverse kinematic problem. Forces $\vec{\mathbf{R}}$ and $\vec{\mathbf{M}}_{\mathbf{R}}$ depending on the state parameters are determined from equations (11). On the other hand, these forces are the resultant spatial forces of the reaction forces of six actuators, therefore they can be determined from the kinetostatic equilibrium equations of the system of forces applied to the platform

$$\sum_{n=3}^{n=8} N_{nx} + R_x = 0; \quad \sum_{n=3}^{n=8} N_{ny} + R_y = 0;$$
$$\sum_{n=3}^{n=8} N_{nz} + R_z = 0; \quad \sum_{n=3}^{n=8} M_x(N_n) + M_{Rx} = 0; \qquad (18)$$
$$\sum_{n=3}^{n=8} M_y(N_n) + M_{Ry} = 0; \quad \sum_{n=3}^{n=8} M_z(N_n) = 0.$$

Thus, from the system of equations (18), thrusts N_i *(i=3,…,8)* are determined for actuators, which are caused by forces $\vec{\mathbf{R}}$ and $\vec{\mathbf{M}}_{\mathbf{R}}$ effecting the WB. At the same time, deformation values of springs depending on the state parameters are known. Values of spring rate and preload are determined based on additional conditions; namely based on the fact that at the end of the forward stroke, elastic forces of the dampers' springs balance the effect of external forces (when the preload is equal to zero).At the same time, it is assumed that all damper springs have the same rigidity, and the maximum inclination angle of the WB during the forward stroke is equal to β.Based on the condition of equality of work of external forces and elastic forces of the springs determine the spring rigidity

$$k = \frac{2 \cdot M_S(F_1, F_2, G) \cdot \beta}{\sum_{i=3}^{i=8} \Delta l_i^2}, \qquad (19)$$

where $M_S(F_1, F_2, G)$ is the work of external forces applied to the WB when turning to an angle β around the mass center; ᵢ- is spring deformation of *I* damper when the WB turns to an angle β (it is established by solving the inverse kinematic problem for the manipulator at the specified angle α).The preload value is established from the fact that during the return stroke of the WB turns at an angle $\beta \le \varphi_1 \le 2\beta$. At the same time, we can also proceed from the condition of equality of works

$$M_S(F_1, F_2, G) \cdot \varphi_1 = k \sum_{i=3}^{8} [(\Delta l_i / 2 + l_{ic}) \Delta l_1]. \qquad (20)$$

Algorithm of the control system in the real time scale determines the value of the preload l_c of the spring of *i* damper found in the equation (20), and required for the return stroke of the working body. Therefore, cyclic movement of the WPS working body is endured.

4. Description of the Design and the Principle of WPS's Operation using the Demonstration Model as an Example

To confirm the functionality of sail WPS, we have produced the working model of WPS presented in Figure *6* that differs from the WPS presented in work [19] with different number of air-inflated sails. In Figure *7*, manipulator transformer for illustrative purposes is presented separately. Here the fixed platform 1 of the parallel manipulator SHOLKOR is connected to the upper platform 2 by six actuators 3. Each rod of the rod-cylinder connection of actuators 3 is linked to the linear power generator rotor 4 that generates electric current registered by the microammeters block 7. The upper platform 2 (Fig.7) of the manipulator is rigidly connected by the mast 5 with toroidal sails 6. Under the drag and lift force, the sail performs spacial cyclic movements depending on the wind direction and speed. In rod-cylinder connection, elastic members in the form of coil springs are installed.

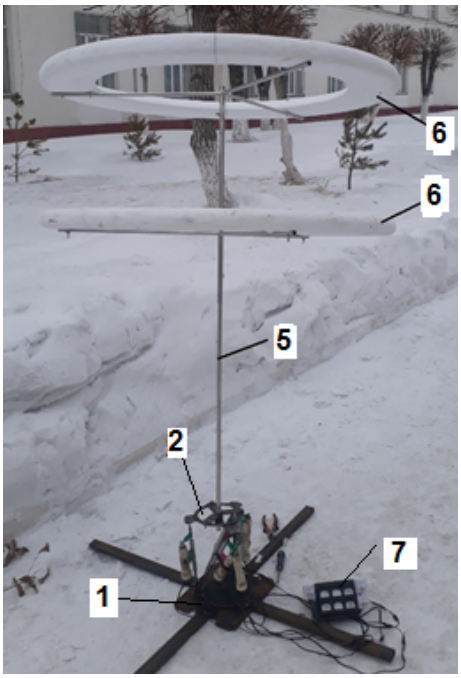

Fig.6. The Demonstration Model of the WPS with a Swinging Working Body

Thus, manipulator additionally performs the functions of the active damping device. The WB moves under the wind gusts and returns to its initial position under the action of damping forces. The working model showed that the shape of the sail in the form of a torus enables the WB's cyclic movement, and increase in the number of sail allows decreasing the dimensions of each sail. With a wind gust, the mastwith the sail deflects at a certain angle, at which the airflow breakdown from the sail occurs. As a result, the impact of the airflow decreases and the WB returns to its initial position under the action of damping forces of the parallel manipulator. With the help of the operating demonstration model, we established that the new, sail WPS differs from existing turbine WPSs by following:

- has cyclically moving WB, in which the sail surface area, flowed around by the air, changes automatically. Due to this the WPS generates electric power of a specified capacity with wind speed of 2.5 m/s to hurricane speed;
- to transform the movement of the WB under the action of wind into an "organized" mechanical movement, the six-degree-of-freedom parallel manipulator SHOLKOR is used, which allows the WPS to function irrespective of the wind direction;
- the parallel manipulator is simultaneously an active special damper, damping capabilities of which are automatically controlled depending on the wind speed to ensure the cyclic movement of the WB.

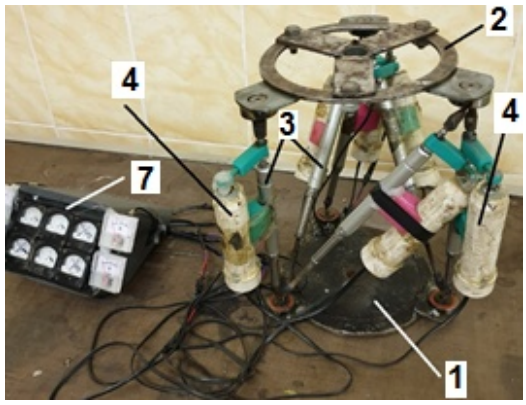

Fig.7. A prototype of WPS of the parallel manipulator

5. Conclusion

In conclusion, we would like to note that this article contains date required for creating and implementing the new automatically controlled sail wind power station having opportunity to generate electric power with low wind speed. The article justifies the sail parameters for the new WPS by the method of computer modeling and

experimental research in wind tunnel. To design and research the sail WPS, the mathematical apparatus based on state equations. Calculations made for the WPS of the given capacity has shown that the sail WPS due to simultaneous effect on the sail by the resistance force and lifting force, converts wind energy more efficiently. It is shown that the algorithm built using the created mathematical apparatus allows selecting the required parameters of the parallel manipulator, and of the active damping device controlled with the help of changing the springs preload. The paper describes the working demonstration sample of the new sail WPS with working body performing cyclic movements. The offered sail wind power station due to its capabilities in efficient energy conversion can significantly expand the application field of the wind sources of renewable energy.

References

[1] M. H. Baloch, J. Wang, G. S. Kaloi, "A Review of the State of the Art Control Techniques for Wind Energy Conversion System", International Journal of Renewable Energy Research, vol. 6, no. 4, pp. 1276-1295, 2016. (Article)

[2] K. S. P'yankov, M. N. Toporkov, "Mathematical modeling of flows in wind turbines with a vertical axis", Fluid Dynamics, vol. 49, pp. 258, 2014. (Article)

[3] R. Gasch, J. Twele, "Langer Grundlagen Windkraft, Entwurf, Planung und Betrieb", Springer vol. 23, pp. 599, 2016. (Article)

[4] S. Apelfröjd, S. Eriksson, H. Bernhoff, "A Review of Research on Large Scale Modern Vertical Axis", Wind Turbines at Uppsala University Energies, vol. 9, pp. 570, 2016. (Article)

[5] A.J. Buchner, M.W. Lohry, L. Martinelli, J. Soria, A.J. Smits, "Dynamic stall in vertical axis wind turbines: comparing experiments and computations", J. Wind Eng. Ind. Aerodyn. Vol. 146, pp. 163-171, 2015. (Article)

[6] H. U. Banna, A. Luna, Sh. Ying, H. Ghorbani, P. Rodriguez, "Impacts of wind energy in-feed on power system small signal stability", 3rd International Conference on Renewable Energy Research and Applications (ICRERA), Milwaukee, WI, USA , pp. 615-622, 19-22 Oct. 2014 . (Conference Paper)

[7] A. Harrouz, I. Colak, K. Kayisli, "Energy Modeling Output of Wind System based on Wind Speed", in the International Conference on Renewable Energy Research and Applications (ICRERA), Brasov, Romania, pp. 63-68, 3-6 November, 2019. (Conference Paper)

[8] S. A. Akdağ, Ö. Güler, E. Yağci, "Wind speed extrapolation methods and their effect on energy generation estimation", in the International Conference on Renewable Energy Research and Applications (ICRERA), Madrid, Spania, pp. 428-430, 20-23 Oktoberber, 2013. (Conference Paper)

[9] C. J. Bai, W.C. Wang, "Review of computational and experimental approaches to analysis of aerodynamic performance in horizontal-axis wind turbines", Renewable and Sustainable Energy Reviews, vol. 63, pp. 506-519, 2016. (Article)

[10] M. Holl, P.F. Pelz, M. Platzer, "Analytical method towards an optimal energetic and economical wind energy converter", J. Energy, vol. 94, pp. 344-351, 2016. (Article)

[11] US20140341736A1, Sail wind turbine, November 2014. (Standards and Reports)

[12] M. M. Hussein et al., "Control of a grid connected variable speed wind energy conversion system," in the International Conference on Renewable Energy Research and Applications (ICRERA), Nagasaky, pp. 1-5, Japan, 11-14 Nov. 2012. (Conference Paper)

[13] O. Kiymaz , T. Yavuz, "Wind power electrical systems integration and technical and economic analysis of hybrid wind power plants", in the IEEE International Conference on Renewable Energy Research and Applications (ICRERA), Birmingham, UK, pp. 158-163, 20-23 Nov. 2016. (Conference Paper)

[14] K. V. Wong, "Land-Sail Vehicle to Generate Electricity", J. Energy Resour. Technol. vol. 137(1), 124-129, September 2014. (Article)

[15] M. Platzer, J. Young, N. Sarigul-Klijn, "Renewable Hydrogen Production Using Sailing Ships". J. Energy Resour. Technol vol. 136(2), pp. 135-140, 2014. (Article)

[16] US 2013 0181458A1, System for converting wind energy, Jul.18, 2013. (Standards and Reports)
[17] J.C. Cajas, M. Zavala, G. Houzeaux, E.Casoni, M.Vázquez, C. Moulinec and Y. Fournier, "Fluid Structure Interaction in HPC Multi-Code coupling", in the Fourth International Conference on Parallel, Distributed, Grid and Cloud Computing for Engineering (PARENG15), Dubrovnik (Croatia), pp 24-27, March 2015. (Conf. Paper)
[18] K.S. Sholanov, Power plants (variants) on the basis of parallel manipulator, WO/2018/147716, 16.08.2018.(St. and Rep.)
[19] K.S. Sholanov, K. Abzhaparov, B. Mirzabaev, "Justifying and choosing parameters of the wind power installation with an automalically controlled sailing working body", Journal Energy Web and Information Technologies, vol. 6, pp. 1-8, July 2018. (Article)
[20] K.S. Sholanov, Platform robot manipulator, WO/2015/016692, 05.02.2015. (Standards and Reports)
[21] C.D. Harris. A matrix of family related airfoils, NASA supercritical airfoils, NASA TP2969, Langley, 1990, pp.72. (Book Chapter)
[22] V. Quaschning, Understanding Renewable Energy System, 436 B/W illustrations Earthscan London, pp.406 .2016. (Book Chapter)
[23] D.A. Spera and T.R. Richard, "Modified power law equations for vertical wind profiles", NASA Lewis Research Center, Wind Characteritics and Wind Energy Siting Conference sponsored by the U.S. Department of Energy, the American Meteorological Society, and the Pacific Northwest Laboratory Portland,Oregon, 19-21 June 1979. (Standards and Reports)
[24] F. Csaki, Nonlinear, Optimal and Adaptive Systems, Budapest, 1972, pp.423. (Book Chapter)
[25] K. Fu, R. Gonzalez and C.S.G. Lee, Robotics: Control, Sensing, Vision and Intelligence, New York:McGraw-Hill, pp. 580, 1987. (Book Chapter)
[26] J.P Merlet, Parallel Robots, Springer Publishers, Dordrecht, pp.332, 2006. (Book Chapter)
[27] K.S. Sholanov, Spatial damping system, Patent №332, Electronic bulletin 16.08.2017. (Standards and Reports)
[28] J.K. Vandiver. "Damping Parameters for flow-induced vibration", Journal of Fluids and Structures, vol. 35, pp. 105-119, 2012. (Article)